Bioelectrochemistry 144 (2022) 107999

Contents lists available at ScienceDirect

Bioelectrochemistry

journal homepage: www.elsevier.com/locate/bioelechem

Assessment of pesticide induced inhibition of *Apis mellifera* (honeybee) acetylcholinesterase by means of N-doped carbon dots/BSA nanocomposite modified electrochemical biosensor

Sehrish Bilal [a,c], Amtul Jamil Sami [a,b,*], Akhtar Hayat [c,*], Muhammad Fayyaz ur Rehman [d]

[a] School of Biochemistry and Biotechnology, University of the Punjab, Lahore 54000, Pakistan
[b] Center for Biosensor Research and Development (CBRD), University of the Punjab, Lahore 54000, Pakistan
[c] Interdisciplinary Research Center in Biomedical Materials (IRCBM), COMSATS University, Islamabad, Lahore Campus, Lahore 54000, Pakistan
[d] Institute of Chemistry, University of Sargodha, Sargodha, Sargodha 40100, Pakistan

ARTICLE INFO

Article history:
Received 9 September 2021
Received in revised form 4 November 2021
Accepted 9 November 2021
Available online 13 November 2021

Keywords:
Carbon dots
BSA
Graphitic pencil electrode (GPE)
Acetylcholinesterase
Honey bee
Diazinon
Docking

ABSTRACT

This work describes the development and optimization of an electrochemical method to evaluate pesticide induced inhibition of honey bee (*Apis mellifera*) acetylcholinesterase (AChE) by means of acetylcholinesterase biosensor. The inhibition assay was based on the detection of changes in electrochemical activity of the enzyme caused by pesticide. As transducer, nitrogen doped carbon dots BSA (N-CD/BSA) nanocomposite electrodeposited on pencil graphite electrode was used to covalently immobilize AChE. The as-synthesized nanocomposite and fabricated electrodes were characterized for the structural, functional and electrochemical properties. Nanocomposite promoted the electron transfer reaction to catalyze the electro-oxidation of thiocholine and a large current response was obtained by cyclic voltammetry at 0.77 V, indicating successful immobilization of AChE. The sensitivity of Diazinon, an OP insecticide, for honeybee AChE was tested under optimal conditions and a linear response ranging 10–250 nM was obtained with a detection limit of 8.9 nM, and sensitivity 9 uA/nM/cm^2. The method showed a good operational reproducibility and selectivity of biosensor. Further, the molecular docking provided additional support to the experimental data suggesting irreversible nature and contact toxicity of the pesticide for honey bee AChE. The developed biosensor has proved useful for the diazinon detection in wheat samples with 99% recovery rate.

1. Introduction

With the consumption of so many novel pesticides, the recent interest of food safety, aside from detecting the trace amounts of pesticides in the contaminated environment, has moved towards determining the impact of these pesticides on non-target organisms such as bees, ants, wasps, termites etc. which play a significant role in maintaining our ecosystem through involvement in pollination, predation, seed dispersal, soil turnover and decomposition etc. Besides it will also help us to select the most efficient pesticides with low residual toxicity to non-target organisms [1,2].

The toxicity of pesticides depends on their ability to target an enzyme Acetylcholinesterase (AChE), by irreversibly modifying the serine residue in the catalytic triad of the enzyme, thus blocking the transmission of nerve impulse that results in mortality of insects. The extent of enzyme inhibition by different pesticides is distinct, which can be used as an indicator to determine pesticide sensitivity to target insects [3]. Previously, various qualitative and quantitative methods have been utilized based on inhibition assays to investigate sensitivity of pesticides [4,5]. Though these methods are reliable but they require complex procedures, pretreatment steps, expensive equipment, high amount of enzyme, and possess altered substrate specificities, which greatly limit their practical applications [6].

Currently, a great deal of research has been focused on enzyme based electrochemical biosensors, using AChE as bioreceptor. This method involves a simple procedure, low cost, rapid response and high test sensitivity, which makes it an effective platform for pesticide sensitivity investigation in insects [7–11]. The present research has focused on the evaluation of pesticide sensitivity to beneficial insects in order to come up with a simplified method

* Corresponding authors at: School of Biochemistry and Biotechnology, University of the Punjab, Lahore 54000, Pakistan (A.J. Sami).
E-mail addresses: sehrishbilal@cuilahore.edu.pk (S. Bilal), amtul.ibb@pu.edu.pk (A.J. Sami), akhtarhayat@cuilahore.edu.pk (A. Hayat), muhammad.fayyaz@uos.edu.pk (M. Fayyaz ur Rehman).

https://doi.org/10.1016/j.bioelechem.2021.107999
1567-5394/

to assess the impact of pesticide exposure on the health and well-being of non-target organisms such as honeybees.

Apis mellifera (Hymenoptera: Apidae) or western honeybees, are striking creatures for their social behavior and essential part they play in global ecology by pollination. They are very important group of eusocial insects responsible for pollination of about 35% of all agricultural crops worldwide. The honey bee mediated pollination values about $175 billion worldwide and $17 billion in the United States [12,13]. They act as living terrestrial bioindicators and forage in a wide area for pollination. During foraging, they can collect traces of contaminants such as heavy metals, and pesticides from the surrounding environment, which also contaminates pollens and nectars collected by honeybees. These pesticide residues ultimately pollute colony matrix and cause serious health disorders in pollen bees leading to sudden declines of honey bee colonies termed colony collapse disorder (CCD) [14]. A US national survey of bee pollen reported that only 18% of samples collected from different regions of USA were free from pesticides [15,16]. To tackle these problems the scientific community is actively working on finding greener and sustainable sources to resolve environmental and healthcare issues. Moreover, the food safety legislations within the European Union, covers all legal issues related to the use of chemicals compounds and tolerable levels of their residues in European Union countries and third world countries [17–20]. However, the monitoring of harmful pesticide residues is of great importance. The authors of [21] reported a micro-analytical system to monitor pesticide hazards in honey bees using LC–ESI–MS/MS method. However, electrochemical assay using AChE biosensor to monitor pesticides sensitivity has not been used for this purpose in spite of having potential to be employed as an effective alternate to conventional assays.

A biosensor's sensitivity is greatly determined by its design that can be tuned by unique nanomaterials to create efficient transducer surface for high performance environmental applications. The tremendous properties of functional nanomaterials such as tunable sizes, structures, shapes, crystallinity and porosity allows the fabrication of bio-surfaces which are capable of potential applications [22]. Such smart materials can be used to modify transducer surfaces to improve the sensitivity and specificity of electrochemical test [23,24].

Among the nanomaterials quantum dots and carbon-based nanomaterials have gained much attention for their outstanding optical, mechanical and electronic properties. More recently, carbon quantum dots or carbon nanodots have evolved as new type nanomaterials with the sizes in the range of 1-–10 nm. These are zero dimensional florescent materials possessing sp^2 hybridized carbon atoms having surfaced passivity for oxygen contained functional groups such as hydroxyl and carboxylic groups [25]. Owing to their outstanding optical and physical properties, quantum confinement, good water solubility, biocompatibility and low cost, they are considered ideal candidates for a wide variety of applications in bioimaging, photocatalysis and biosensing [26–28].

To improve the photo-physical properties of CDs, their doping with heteroatoms such as Nitrogen, have been greatly pursued [29]. The nitrogen doped carbon nanotubes have been explored for their incredible electrocatalytic properties and uses in energy storage, oxygen reduction, electrochemiluminisence and biosensors. The nitrogen doping of CDs causes charge delocalization offering tunable optical properties causing high electron transfer capability and improved conductivity. Further. the preeminent intrinsic properties of N-CDs such as high electron transfer, small size, large specific surface area, numerous edge sites and high catalytic activity makes them highly suitable for electrochemical sensing [30]. N-CDs can be easily prepared in single step through bottom up microwave assisted method consuming inexpensive starting materials which produce stable and non-toxic N-CDs with high stability in aqueous medium [31,32].

The carbon quantum dots possess exceptional electronic conductivity but their inherent defects and other factors may hamper their conductivity. Researchers have reported a number of major developments in carbon dots modifications and their applications [33]. The grouping of N-CDs with other functional materials in one microstructure has been exploited in the construction of sensors for various applications. For instance, the authors of [34] designed a ternary heterojunctions composed of BiOCl, $BiVO_4$ and N-CDs which exhibited enhanced photocurrent in a sensor platform for detection of the dopamine. The authors of [32] developed a taurine sensor using ECL properties of the N-CDs. The scientists in [35] utilized N-doped porous Mo_2C nanoflowers to develop a new sensor for monitoring of organophosphorus pesticides. However, the use of the CDs to construct electrochemical sensors for biological and agricultural samples is still under development.

Herein, we report a novel N-CD/BSA nanocomposite where surface functionalities of nanodots were integrated with BSA that provides a non-toxic surface with good chemical stability, high electrical conductivity and numerous active sites to act as ideal catalyst support material with strong affinity for protein fixation without deactivating protein. The nanocomposite was electrodeposited on the pencil graphite electrode providing thin layer of material with high rate of deposition on electrode surface. The honeybee AChE was used in its native environment to ensure its inherent structural stability and activity. The enzyme was covalently immobilized on modified transducer surface which leads to a stable AChE biosensor for study of its inhibition by pesticides. An organophosphate insecticide Diazinon was adopted to validate this proposed method and the results were compared with computational modelling of enzyme with inhibitor to analyze their interaction pattern and binding mechanism. The developed electrochemical method integrating the properties of N-CD/BSA nanocomposite with electrochemical test was sensitive and selective for the interpretation of inhibition sensitivity of diazinon associated with honeybee AChE activity.

2. Experimental section

2.1. Reagents

Acetylthiocholine chloride (ATCl), Urea, D- Fructose, Bovine serum albumin (BSA), Chloroacetic acid, Sodium hydroxide, Potassium ferrocyanide ($K_4[Fe(CN)_6]$) and Potassium ferricyanide ($K_3[Fe(CN)_6]$) and Diazinon were supplied by Sigma-Aldrich Corporation, USA. NHS (N-hydroxysuccinimide) was obtained from CovaChem, USA. EDC (1-Ethyl-3-(3-dimethylaminopropyl) carbodiimide) and MES (4-morpholinoethanesulfonic acid) were obtained from Tokyo chemical company (TCI), Japan. All chemicals were of analytical standard and used without purification. For aqueous solutions water from a Millipore Milli-Q system was used.

2.2. Synthesis of N-CD

Carbon nanodots associated with amine group (N-CD) were synthesized by a fast and controlled microwave assisted heating method originally proposed by [32] which produced CDs peripherally abundant in nitrogen functional groups. Briefly, 1 mM D-Fructose and 3 mM Urea was mixed in 10 ml of DI water and agitated for 10 min to get a homogenous solution. The solution was heated for 4 min in a domestic microwave oven (750 W) until a dark brown caramelized solid. The solid was incubated at 60 °C for one hour, re-dissolved in 20 ml of DI water and was left in dark for 24 h at RT. After that the solution was stirred for 1 h and cen-

trifuged at 10,000 RPM for 30 min to get rid of the large sized particles. The obtained supernatant was filtered through 0.22 μm syringe filter to obtain the N-CD solution. The as prepared N-CDs were stable in solution at 4 °C for several weeks.

2.3. Carboxylation of N-CD and formation of N-CD/BSA nanocomposite

The amine rich carbon dots were further functionalized with carboxylic acid functional groups by mixing 5 ml solution of as prepared N-CDs with 0.5 mM chloroacetic acid under highly alkaline environment to convert OH– groups on N-CDs surface to carboxyl functional groups. The acidic solution was thoroughly mixed with N-CDs by sonication for 3 h. The functionalized N-CD/BSA nanocomposites were prepared by mixing N-CD-COOH solution with 0.05% (w/v) of BSA and the solution was left overnight for stirring at 4 °C.

2.4. Instruments

UV–Vis measurements were performed on a Lambda-35 spectrophotometer (PerkinElmer, America) in the range of 200–800 nm. Fluorescence (FL) spectra were collected with Cary Eclipse fluorescence spectrophotometer (Agilent technologies, USA) equipped with a 1 cm × 1 cm quartz cuvette. The Fourier Transform infrared Spectroscopy (FTIR) was performed on Thermo Fischer Scientific (Nicolet 6700, USA) spectrometer at scan range 600–4000 cm^{-1}. For the photoluminescence (PL) measurement of material Xe Lamp source F7000 Hitachi Spectrometer was used and excitation wavelength was set at 488 nm. Cyclic voltammetry was carried out on AMEL Electrochemistry Potentiostat (Model 2551) using Ag/AgCl reference and platinum wire counter electrode. The working electrode was Pencil graphite electrode (PGE) (diameter: 0.5 mm; length: 60 mm) from Staedtler, Germany. For biosensor current measurements potential swept across 0.2 V to 0.9 V in 0.1 M PBS (pH = 7.4). The Electrochemical impedance spectroscopy (EIS) was carried out using 2700 Z-Pulse by AMEL Electrochemistry at a frequency range from 0.1 Hz to 0.1 MHz.

2.5. Preparation of AChE/N-CD/BSA/PGE biosensor

To prepare acetylcholinesterase based biosensor AChE from *Apis mellifera* was used to immobilize on N-CD/BSA modified pencil graphite electrode. The crude extract of 80 mg insects was prepared by homogenizing in 0.1 M PBS (pH = 7.4). After centrifugation, the resulting supernatant was used as source of enzyme. 5 μl of AChE extract was mixed with 1.5 μl of 100 mM EDC/NHS/MES buffer solution for the activation of carboxyl functional groups [11]. For biosensor fabrication, the electrodes were cleaned to oxidize or reduce the impurities by electrochemical pretreatment through consecutive cyclic voltammetry scans in 0.5 M H_2SO_4 potential in the range of −1.5 V to +1.5 V. Then the electrochemical modification of PGE with N-CD/BSA nanocomposite was performed with linear sweep voltammetry (LSV) using 0.5 M acetate buffer as electrolyte by sweeping potential between 0 and 1 V at 50 mVs^{-1}. The amino group on the electrode surface was conjugated to carboxyl groups of AChE, by immersing the modified electrode in AChE/EDC/NHS/MES solution for 45 min at 30 °C to covalently immobilize enzyme through amide bond formation. The fabricated electrodes were washed with PBS (0.1 M, pH = 7.4) carefully, dried and used for further electrochemical measurements. A general scheme for the steps involved in the fabrication of biosensor is presented in Scheme.1.

2.6. Electrochemical measurement of modified electrodes

For electrochemical measurement of the biosensor, cyclic voltammograms were recorded using 5 mM [1:1] $K_3[Fe(CN)_6]$/$K_4[Fe(CN)_6]$ solution in 0.1 M KCl as an electrolyte and to determine analytical response of the developed biosensor the CV was recorded in response to acetylthiocholine chloride (ATCl) in 0.1 M PBS (pH = 7.4), at potential ranging from 0.2−0.9 V with 50 mVs^{-1} scan rate. Negative and positive controls were run alongside and expected oxidation peak of thiocholine was observed in each electrode. For each measurement substrate containing buffer was replaced with fresh one and each electrode was used only once.

For inhibition studies, same procedure was employed including pre-incubation of electrodes with Diazinon with gentle stirring which helps in particle dispersion and improves the coating quality. The incubation time was optimized by immersing the integrated bioelectrodes in pesticide solution for 5 to 60 min, and optimum incubation time for inhibition was recorded. The work utilized a single electrode system and freshly prepared individual bioelectrode has been used that has not been previously inhibited by the pesticide, to record current response for each concentration. CV was recorded afterwards and percentage inhibition was calculated by the following equation: [36].

$$I\% = \frac{I_0 - I_1}{I_0} \times 100 \quad (1)$$

where I_0 is the oxidation peak current for thiocholine produced by the hydrolysis of AChE, and I_1 is the oxidation peak current for thiocholine in the presence of inhibitor (Diazinon).

The calibration curve for Diazinon was formed and LOD, Michaelis Menten Kinetics and sensitivity of biosensor was also calculated.

2.7. Ligand preparation and protein structure modelling

The structure for Diazinon was attained from PubChem (*https://pubchem.ncbi.nlm.nih.gov*) in SDF format (CID: 3017). The homology models for Am-AChE (*Apis mellifera*) and Tc-AChE (*Tribolium castaneum*) was obtained using PDB templates with an identity of above 50% (Table S1). The homology model for AChE was built through YASARA (Yet Another Scientific Artificial Reality Application) Structure version 20.1.18 [37] following by structure refinement using loop region optimization and steepest descent, simulated annealing minimization as described in a previous study [38]. All models were further validated using PROCHECK server (*http://www.ebi.ac.uk/thornton-srv/software/PROCHECK/*), VERIFY 3D server (*http://services.mbi.ucla.edu/Verify_3D/*) and Ramachandran plot distribution.

2.8. Docking study

For diazinon molecular docking against Am-AChE and Tc-AChE, YASARA Structure software version 20.1.18 [37] with a modified AutoDock LGA algorithm and an AMBER03 force field was used. To improve the accuracy of the process 100 global docking runs were obtained, rescored and analyzed for dissociation constants, binding energy calculations and active site mapping as described by [11]. PyMol, and LigPlus [39] were used to map the ligand–protein interactions.

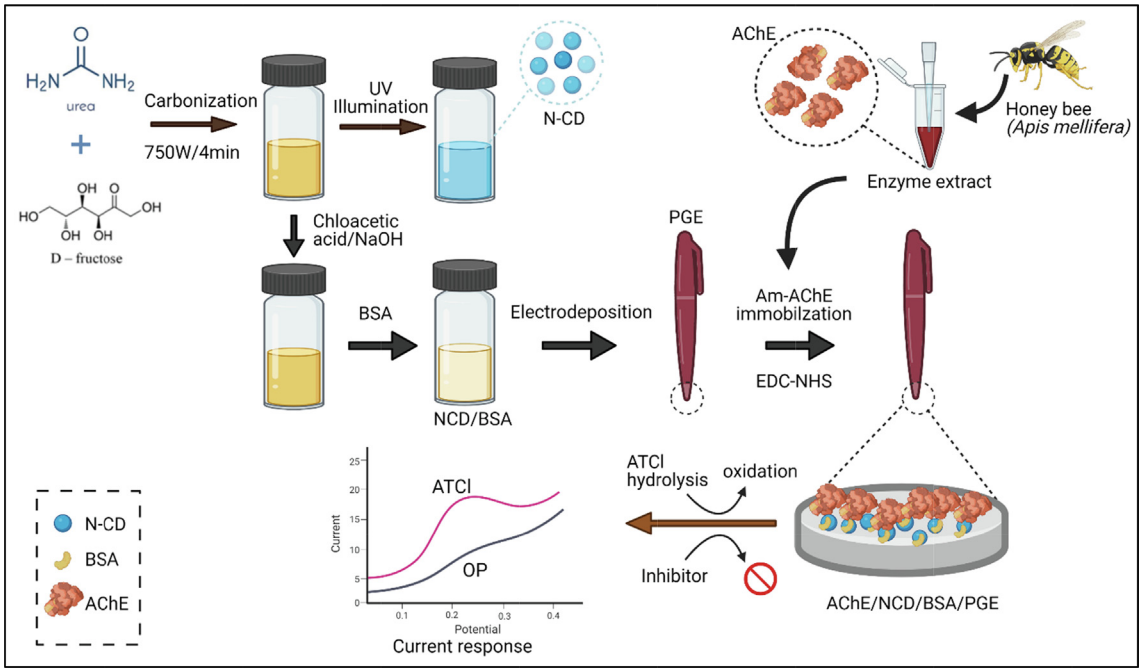

Scheme 1. Schematic illustration for the preparation of N-CD/BSA composite and fabrication of AChE/N-CD/BSA/PGE biosensor for the monitoring of diazinon poisoning. Graphics created with *biorender.com.*

3. Results and discussion

3.1. Characterization of N-CD and N-CD/BSA nanocomposite

The optical properties of as-prepared N-CD were explored through UV–visible absorption spectroscopy and florescence emission spectroscopy by varying excitation wavelengths. As shown in Fig. 1A, the absorption spectrum of N-CD in aqueous medium showed absorption bands at 272 nm and 320 nm. The band at 272 nm represent n-π* transition characteristic due to C=O bonds which are covalently bonded to the outer sp^3 carbons of the carbon dots. Besides, a strong absorption was obtained near to the visible region at around 320 nm which is attributed to the n-π* electronic transition of C=O and C—N bonds originated due to excited defect surface state formation by the addition of nitrogen heteroatoms, which makes the surface groups of N-CDs more heterogeneous [32,40,41]. The change in absorption spectrum was also observed after incorporation of BSA with N-CDs. A characteristic absorbance band of BSA was observed at around 280 nm with increased absorption intensity. The increase in absorbance intensity is probably due to the conformational change in peptide coiled backbone upon complexation with N-CDs which further confirms hydrophobic micro-environment around peptide backbone [42]. The aqueous solution of N-CDs appeared light brown under normal light while showed blue florescence when exposed to UV light as shown in the inset of Fig. 1A, therefore when florescence emission spectra of aqueous solution N-CD was recorded, maximum emission was observed at 400 nm at the excitation wavelength of 320 nm. It is known that the florescent emission of N-rich carbon quantum dots is sensitive to changes in excitation wavelength. The resultant emission spectra are broad and random, usually falls between 400 and 500 nm, which is due to the presence of several absorbing and emitting centers around N-CD attributed to their different sizes causing radiation dispersion [32,43,44]. The same effect can be seen in Fig. 1B that with the increase in excitation wavelength, a red shift in emission spectra occurs attributed to the characteristic bathochromic effect of N-CD along with a subsequent decrease in florescent intensity. The same effect was observed in the N-CD/BSA nanocomposite, however the emission spectra further shifts forward due to the presence of BSA with N-CDs (Fig. 1C), suggesting a ground state complex formation which results in change in conformation around Trp residues of BSA.

Currently, a great deal of research has been done to study PL of carbon dots which is considered a characteristic of C-dots used in photocatalysis [26,45]. The material is known to possess uniform size with good luminescence, high stability, and excitation related photoluminescence (PL) property. Fig. 1D shows the PL spectra for the as prepared N-CD and N-CD/BSA nanocomposite at excitation wavelength of 488 nm. It is eminent that the UV excitation has shorter wavelength than emission. It has been reported that the emission at 385 nm occurs due to the extended conjugation of π-electron domains in the C-dots and presence of surface trap states (STS) results in strong emission at 460 nm which indicates electronic nature of carbon dots [46]. Noticeably, the absorption intensity of N-CD/BSA nanocomposite is higher and the absorption edge is somewhat shifted towards red in the visible region in contrast to N-CDs. A large difference in absorption characteristics indicates the existence of BSA on the surface of N-CDs, as the presence of BSA offers multiple functional groups such as thiol, —OH, —COOH and $—NH_2$, which helps in passivating the inherent electronic defects of N-CDs. Moreover the high surface energy and reactivity of BSA allows binding of small sized N-CDs and produce a synergistic effect between N-CD and BSA causing a more obvious increase in PL intensity after formation. It can also be conferred that the nanocomposite may have visible light absorption and thus result in the production of more electron hole pairs as indicated by higher PL intensity of nanocomposite material [47,48].

Fourier transform infrared (FTIR) spectroscopy was executed to determine the presence of functional groups on the surface of N-CDs depending on their starting materials. The FTIR spectra shown in Fig. 2A shows a broad band as opposed to the starting materials (Urea and Fructose) at 3350 cm^{-1} ascribed to the vibrational stretching of O-H and N-H bonds, signifying the presence of hydroxyl and amino functional groups on the edges of N-CDs, which

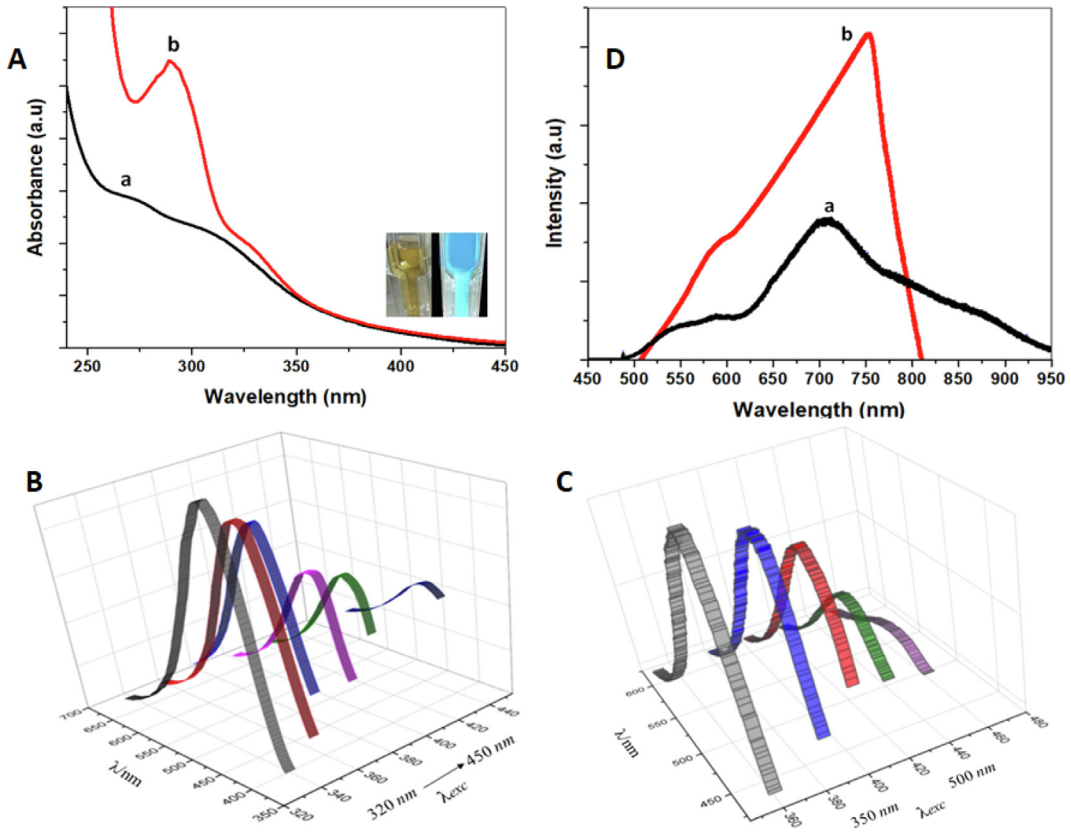

Fig. 1. (A) UV–Vis absorption spectra of the Nitrogen doped CDs (a), and N-CD/BSA (b), inset: optical images taken under white light (left) and under UV light (right). (B) The Fluorescence Emission spectra obtained at distinct excitation wavelengths of N-CD in aqueous solution (320–450 nm) and (C) N-CD/BSA (350–480 nm). (D) PL spectra of as prepared N-CDs (a) N-CD/BSA (b).

makes them soluble in aqueous solvents [32,44]. The carbogenic core of N-CDs results in absorption bands at around 1642 cm^{-1} and 1575 cm^{-1} which correspond to the vibrational stretching of C═O and skeletal N-H bending, moreover the peak at 1410 cm^{-1} arise due to stretching of C—N amide bonds [49]. The presence of these functional groups greatly improve their modification with other inorganic or organic materials, which makes them an excellent choice to use as support materials or signal transducers in development of electrochemical sensors with enhanced electrocatalytic efficiency. Herein the as prepared N-CDs were integrated with BSA and FTIR spectra of N-CD/BSA nanocomposite was also recorded. The characteristic bands of pure BSA can be seen in Fig. 2A at 1642 cm^{-1}, 1536 cm^{-1} and 1240 cm^{-1} attributed to amide I having high α helix content, amide II band and amide III due to antiparallel β sheet vibrations respectively. However in the N-CD/BSA nanocomposite a broad absorption band at 3290 cm^{-1} belong to vibrational stretching of O—H and N—H bonds of NCD whereas the intensity of characteristic BSA bands reduced upon incorporation of BSA with NCD indicating a reduction in α helix content of BSA after binding with nanodots. The changes in the peak positions in the FTIR spectrum indicate sufficient cross-linking between BSA and NCD [47].

3.2. Electrochemical characterization of integrated electrodes

The electro-oxidation of material at different steps of electrode modification was characterized by LSV and the current at the electrodes was measured by sweeping potential from 0 to 1 V between the working and the reference electrode at a scan rate of 50 mVs^{-1}, using acetate buffer pH 4.5. The oxidation peak current of N-CD and N-CD/BSA can be seen in Fig. 2B, which shows a high magnitude of peak current in case of N-CD deposition suggesting high electron transfer and conducting nature of N-CDs, whereas the magnitude of peak current decreases for N-CD/BSA electrode revealing immobilization of BSA on N-CD electrode. Moreover the oxidation current for N-CDs modified with carboxyl groups moved more towards negative due to hindrance in electron flow due to negative charge of COO^- functional groups [50,51]. Furthermore, the electrochemical behavior of prepared materials was investigated by cyclic voltammetry (CV) and electrochemical impedance spectroscopy (EIS). For comparison, bare PGE, N-CD/PGE, N-CD-COOH/PGE and N-CD/BSA/PGE were prepared in the same condition. Fig. 2C shows the CV responses of bare PGE (a, black), N-CD/PGE (b, green), N-CD-COOH/PGE (c, blue) and N-CD/BSA/PGE (d, red) modified electrodes which was carried out in 10 ml of [1:1] $K_3[Fe(CN)_6]/K_4[Fe(CN)_6]$ solution in 0.1 M KCl. As illustrated, the bare PGE showed weak electro-activity and inconspicuous current peaks. By contrast, the modified PGEs increased the electrochemical signals in different degrees. Notably, N-CD/PGE showed an increase current response with respect to bare PGE, whereas the electrochemical response declined in case of carboxyl group functionalized N-CDs due increased current resistance hampering the transfer of electrons resulting in high impedimetric response, however the N-CD/BSA/PGE exhibited a maximum redox current suggesting the electron transfer kinetics of redox probe is improved after nanocomposite deposition and a most distinguished electroactive response on the surface of electrode was obtained. The results corroborate with the EIS responses as shown in the Nyquist plots in Fig. 2D that the bare PGE showed maximum resistance to current flow as compared to N-CD/PGE and N-CD/BSA/PGE represented a considerable decrease in the diameter of the semicircle at high frequency, which confirms the conductivity

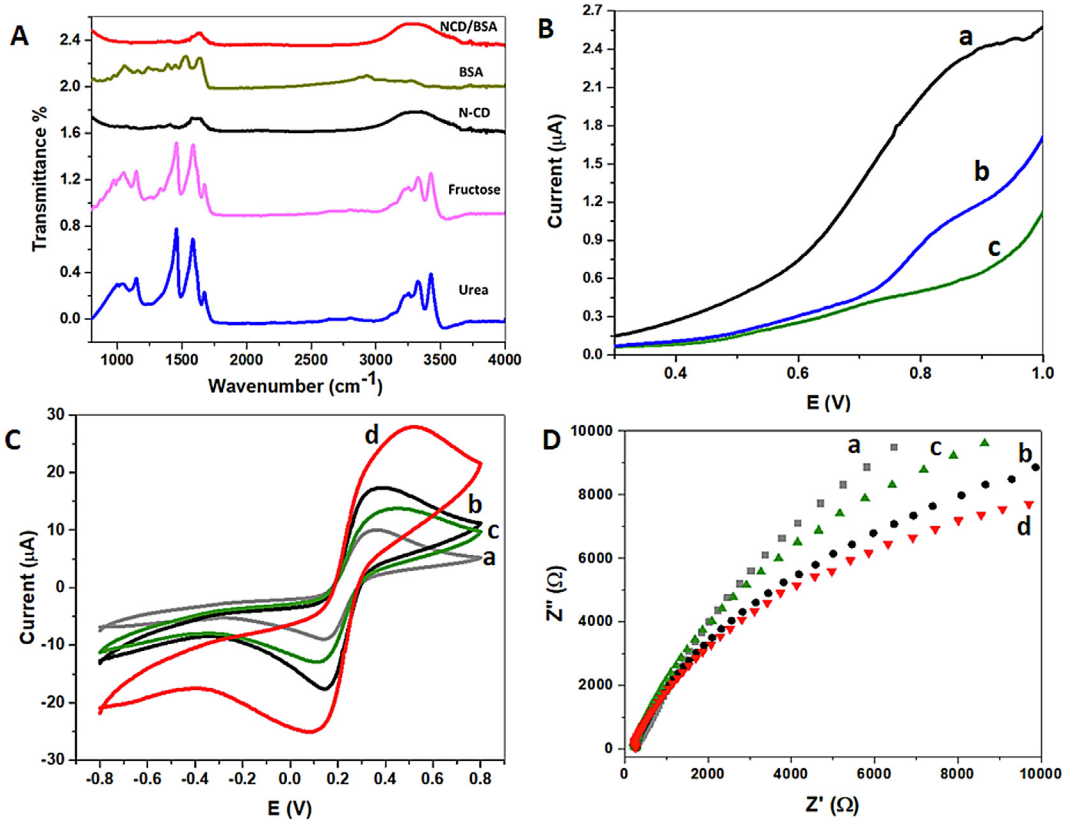

Fig. 2. (A) FTIR spectra of urea, D-fructose, N-CD, BSA and N-CD/BSA. (B) Linear sweep voltammetry at 50 mVs^{-1} for N-CD (a), carboxyl functionalized N-CD/COO^{-} (b) and N-CD/BSA nanocomposite (c) at a potential range from 0 to 1 V. (C) Cyclic voltammograms of bare PGE (a), N-CD/PGE (b), N-CD-COOH/PGE (c) and N-CD/BSA/PGE (d) modified electrodes at 50 mVs^{-1} by sweeping potential across −0.8 to 0.8 V using 5 mM $K_3[Fe(CN)_6]/K_4[Fe(CN)_6]$ solution in 0.1 M KCl as electrolyte. (D) EIS Nyquist plots of bare PGE (a), N-CD/PGE (b), N-CD-COOH/PGE (c), and N-CD/BSA/PGE (d) electrodes.

of the electrode is increased due to the presence of N-CD/BSA nanocomposite on the surface of electrodes, whereas the hindrance increased in case of N-CD-COOH/PGE due to repulsion of negative charges [11].

3.3. Verification of *A. mellifera* AChE immobilization

The success of *A. mellifera* AChE immobilization was verified by recording CV and EIS of enzyme immobilized electrodes. An explicit increase in electron transfer resistance can be envisioned after immobilization of *A. mellifera* AChE on electrode surface. The cyclic voltammogram of AChE/N-CD/BSA/PGE electrode shows a decline in redox current due to insulating nature of enzyme which hampered the transfer of redox probe to electrode surface therefore cause an increase in impedimetric response as compared to N-CD/BSA/PGE, however the current resistance of bare PGE was efficiently reduced after electro-oxidation of BSA. The simultaneous decline of redox current and increase in impedance as shown in Fig. 3, confirms successful enzyme attachment on electrode surface establishing a highly efficient sensing method for organophosphates detection. The presence of BSA in the nanocomposite benefits with providing a biocompatible environment for enzyme and blocks non-specific binding of protein. Further, the EDC/NHS functionalization improved specific interaction of the enzyme with nanocomposite on electrode surface.

3.4. Analytical behavior of AChE/N-CD/BSA/PGE biosensor

Fig. 4 shows the electro-catalytic response of the fabricated biosensor in 0.1 M pH = 7.4 PBS containing ATCl, substrate for AChE. It can be seen that for the negative control electrodes (a, b, c and d), there is no detectable oxidation peak within the detection range. However, in the presence of 6 mM ATCI in PBS solution, a large oxidation peak occurred at AChE/N-CD/BSA/PGE at 0.77 V with 4 μA oxidation current. The results illustrate that the immobilized AChE on N-CD/BSA/PGE electrode is able to catalyze ATCl into electroactive thiocholine (TCh) which generates an obvious oxidation peak. The results depict that the prepared N-CD/BSA provides an ideal biocompatible platform to act as template for efficient AChE immobilization which results in the increase in electrochemical response without disturbing enzyme's natural conformation and catalytic activity.

3.5. Experimental optimization

The experimental conditions to get best performance of proposed biosensor had been optimized. The effect of scan rate on electrochemical performance of biosensor was also studied. Results demonstrate that anodic peak current increased exponentially with increase in scan rate from 10 to 150 mVs^{-1}. The figure shows a linear response between square root of scan rate with anodic peak current with regression equation as Ipa (μA) = 0.0576ν + 0.1366 (mVs^{-1}) and correlation coefficient of 0.9832, which proves a surface controlled process on the surface of modified electrode (Fig. 5A).

The influence of the AChE concentration on the performance of the AChE/N-CD/BSA/PGE electrode was also studied. The electrochemical responses of the modified electrodes were measured after the AChE immobilization on the surface of the modified electrodes. The current response of the AChE/N-CD/BSA/PGE electrode

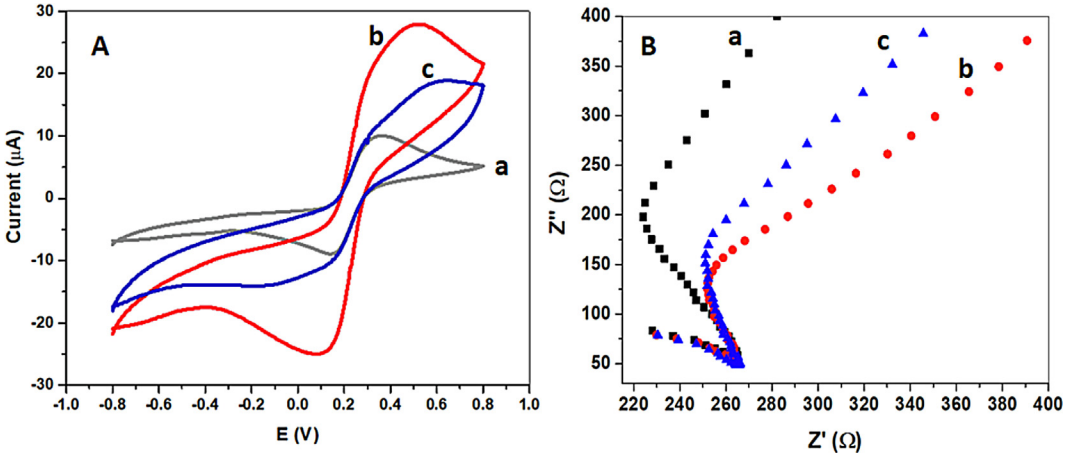

Fig. 3. (A) CV response of bare PGE (a), N-CD/BSA/PGE (b) and *A. mellifera* AChE/N-CD/BSA/PGE (c) modified electrodes at 50 mVs^{-1} by sweeping potential across −0.8 to 0.8 V using 5 mM $K_3[Fe(CN)_6]/K_4[Fe(CN)_6]$ solution in 0.1 M KCl as electrolyte. (B) EIS Nyquist plots of bare PGE (a), N-CD/BSA/PGE (b) and AChE/N-CD/BSA/PGE (c) modified electrodes at a frequency range from 0.1 Hz to 0.1 MHz.

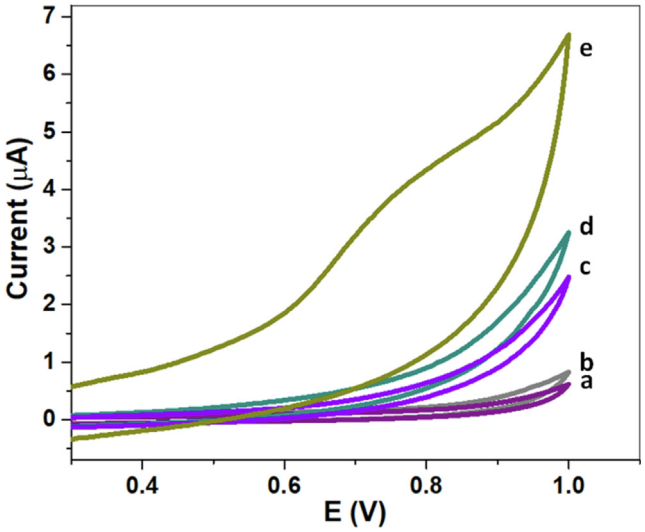

Fig. 4. CV response of as fabricated AChE/N-CD/BSA/PGE biosensor in 0.1 M pH = 7.4 PBS using 6 mM ATCl (e), and negative controls [(a) bare PGE in PBS, (b) bare PGE in PBS containing 6 mM ATCl, (c) N-CD/BSA/PGE in PBS, (d) N-CD/BSA/PGE in PBS containing 6 mM ATCl]. The oxidation peak of thiocholine as produced by hydrolysis of ATCl by AChE appeared at 0.77 V showed good analytical response of prepared biosensor interface.

was maximum when 0.8 $mg\mu L^{-1}$ extract was used. So 0.8 $mg\mu L^{-1}$ crude AChE solution was considered adequate for effective binding to the electrode and optimum current response. Nonetheless, the incubation time of AChE on the surface of the AChE/N-CD/BSA/PGE electrodes was also examined. As shown in Fig. 5B, the current responses of the prepared electrodes increased maximally after 45 min of incubation and slightly declined after that which may be attributed to the physical hindrance provided by the excess of enzyme to the current flow after the saturation point. The 45 min incubation time was enough for the firm immobilization of the AChE on the surface of the electrode, which was selected for further experiments.

Moreover, the inhibition time of the diazinon for the inhibition of AChE was also investigated. As shown in Fig. 5C, the current response of the AChE/N-CD/BSA/PGE electrode showed a sequential increase when the inhibition time in OPs solution extended from 5 min to 30 min and then became constant. The result revealed that after 30 min the inhibition of the enzyme was saturated. Therefore, 30 min inhibition time was adopted for the inhibition experiments.

3.6. Calibration curve of ATCl

One of the most important experimental parameters to determine the bioelectrocatalytic activity and analytical performance of the developed biosensor interfaces is the concentration of substrate. Fig. 6A exhibits the current response of the prepared electrodes when the concentration of ATCl was increased from 1 mM

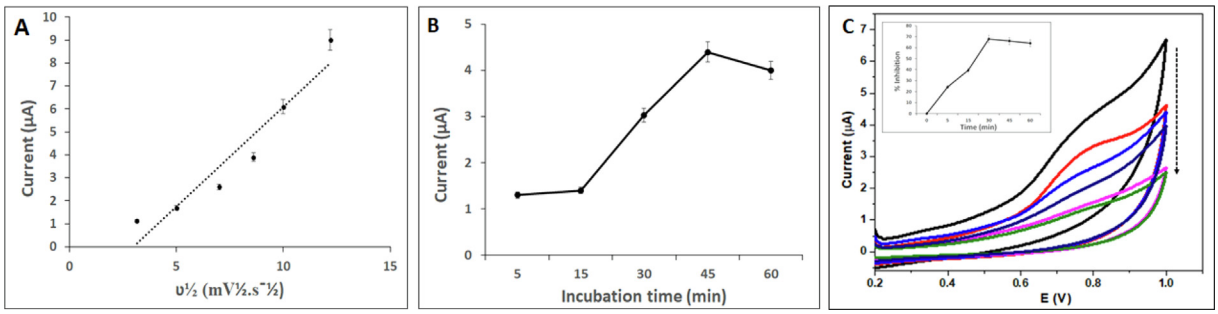

Fig. 5. (A) Plot of square root of scan rate vs. peak oxidation current, where linear equation is Ipa (μA) = 0.0576ν + 0.1366 (mVs^{-1}), and R^2 = 0.9832 (B) Effect of incubation time of Am-AChE enzyme extract on peak oxidation current of thiocholine, (C) Effect of inhibition time on AChE/N-CD/BSA/PGE after exposing with 100 nM of diazinon. Inset shows plot of percentage inhibition of pesticide with time. Error bars represent standard deviation of three readings.

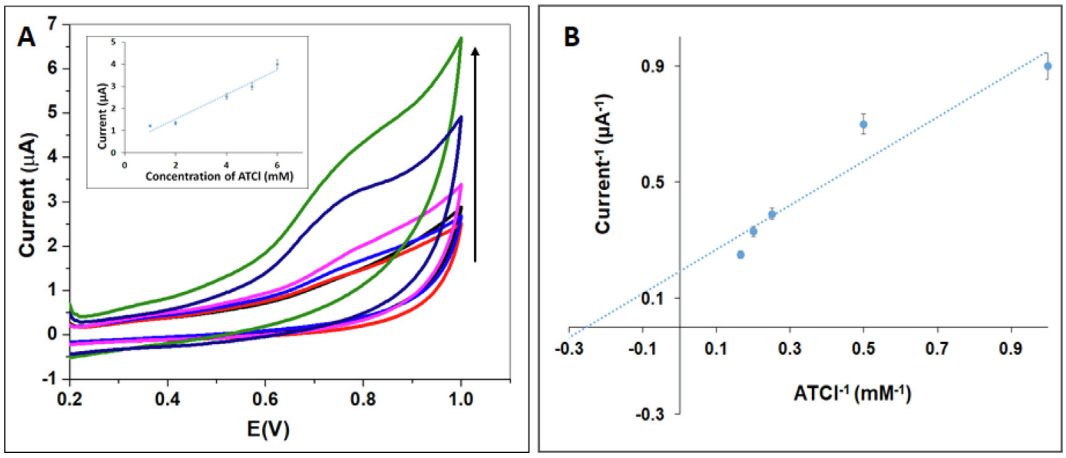

Fig. 6. (A) CV response of AChE/N-CD/BSA/PGE biosensor with increasing concentrations of ATCl in 0.1 M PBS (pH = 7.4) (inset shows the calibration plot of current versus ATCl concentration, with the linear equation as Ipa (μA) = 0.556c + 0.4102, and R^2 = 0.9632 (B) Lineweaver burk plot of Current^{-1}/μA^{-1} vs. ATCl^{-1}/mM^{-1} displaying Michaelis menten kinetics of biosensor, with the linear equation as Ipa (μA) = 0.7582c + 0.1931, and R^2 = 0.9207.

to 6 mM. The greater the concentration of ATCl, the more thiocholine was produced. Subsequently, the enhanced current response was achieved with a linear relationship between the oxidation peak current and the concentration of the substrate and the linear regression equation was given as, Ipa (μA) = 0.556c + 0.4102, with R^2 = 0.9632. When the concentration of ATCl exceeded 6 mM, the current response was almost constant exhibiting the saturation of available active sites of enzyme. So, the concentration of 6 mM ATCl was employed for optimum bioelectrocatalytic behavior AChE/N-CD/BSA/PGE electrodes. The results showed that the catalytic response of the developed biosensor follows Michaelis-Menten kinetics and Lineweaver Burk equation [52] was used to calculate apparent Michaelis-Menten constant (Km^{app}) of the developed biosensor. The Km^{app} for integrated bioelectrodes was computed to be 3.9 mM (Fig. 6B). This value shows a good enzyme kinetic behavior and the obtained Km^{app} value displays a good substrate affinity for a biosensor fabricated with crude enzyme source emphasizing the potential of this method in preparation of a competitive biosensor interface for desired applications. Noticeably, this value is also comparable or smaller than many lately reported AChE biosensors [11,53–55].

3.7. Effect of Diazinon on activity of immobilized AChE

The analytical performance of the deduced biosensor to evaluate the sensitivity of OPs to *A. mellifera* AChE was assessed with diazinon as a model pesticide. The organophosphate is widely used to control insects and mites and is considered quite toxic to honey bees. Fig. 7A illustrates the CV responses in 6 mM ATCl after incubating the integrated bioelectrodes with various concentrations of diazinon. The plot of current versus percentage inhibition gives range from 10 to 250 nM and the limit of detection (LOD) as calculated using standard deviation of the lowest response and slope of the calibration curve, was 8.6 nM. The LOD value and the linear range of the as fabricated biosensor is comparable to various previously reported electrochemical methods proposed for diazinon detection (Table 1). Similarly, the sensitivity of the integrated electrode was found to be 9 μA/nM/cm^2. It can be deduced from the following findings that the as fabricated interface is suitable for detection of diazinon and exhibit a concentration dependent electrocatalytic behavior of the nanocomposite fabricated electrode. The obtained results justify the scope of this study in terms of detection sensitivity and toxicity investigation. It can also be deduced from the results that the activation of detoxification mechanisms of honeybees may restrict enzyme inhibition at very low diazinon concentrations.

3.8. Mechanism of inhibition and inhibition kinetics

The proposed method was also employed to investigate the mechanism of inhibition of *A. mellifera* AChE by diazinon. The mechanism of inhibition and inhibition kinetics can be proficiently determined by double reciprocal plots of $1/I_{pa}$ as a function of 1/[S]. A double reciprocal plot of the enzyme kinetics in the presence and absence of diazinon shows changes in values of Km^{app} corresponding to changes in $Vmax^{app}$. As shown in Fig. 7B, the visual impression of plot confirms non-competitive inhibition of enzyme with diazinon. Technically, the apparent Km computed from Lineweaver Burk equation was 3.9 mM both in the presence and absence of diazinon, whereas whereas Vmax lowered in the presence of diazinon from 5.26 mM/min to 3.9 mM/min, which describes a non-competitive or irreversible inhibition of *A. mellifera* AChE activity by diazinon. These results are supported by literature [62] and it should be noted that the presented platform is equally suitable to study enzyme inhibition kinetics and behavior of insect enzymes in the presence of inhibitors.

3.9. Molecular docking analysis of Diazinon with A. mellifera AChE

Molecular docking analysis is an effective tool to study the interaction between receptor protein and a target ligand. The physicochemical properties of the protein and docking analysis of the inhibitors helps in understanding the binding mode of pesticides in addition to predicting the overall toxicity of the pesticides. In order to find out the structure and function relationship of *A. mellifera* AChE inhibitor, molecular docking was performed. The homology models for *A. mellifera* AChE1 were obtained as described in our previous work [11]. The model validation was done by YASARA z-scores (Table S1), Ramachandran plot and other servers which showed acquisition of good quality homology modelled structure (Fig S1).

Molecular docking shows that Diazinon interacts with honey been acetylcholinesterase. The binding energy of Diazinon for Am-AChE1 was found to be −5.15 kcal/mol and the dissociation constant is 168.2 μM. The Diazinon interact with Am-AChE1 at an allosteric site near the active site gorge of enzyme. The amino acid residues Trp^{116} and Tyr^{385} shows π-π interactions, while Gly^{167} and Tyr^{389} make strong hydrogen bonds with inhibitor, rest

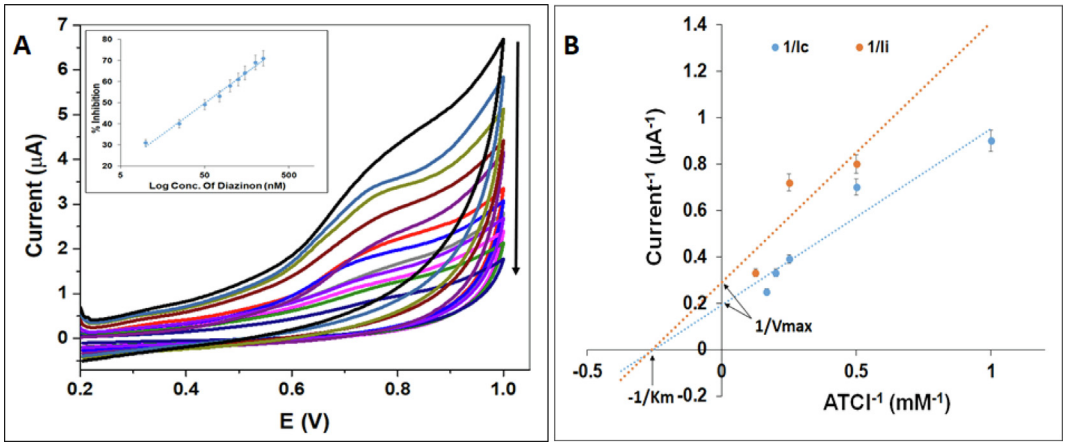

Fig. 7. (A) CV curves of biosensor after incubating with different concentrations of Diazinon in 0.1 M PBS (pH = 7.4) containing 6 mM ATCl: inset shows calibration curve for detection of Diazinon at a linear range of 10–250 nM, with the linear equation as Ipa (μA) = 12.744ln(x) - 0.1327, and R^2 = 0.9917 (B) Lineweaver-Burk plots (1/S vs.1/Ipa) of ATCl with and without diazinon indicating same Km^{app} value and different $Vmax^{app}$ suggesting irreversible inhibition mechanism of *A. mellifera* AChE inhibition by Diazinon.

Table 1
A brief comparison of the proposed biosensor performance with some previous reports of sensors developed for Diazinon determination.

Sr.	Electrode	Linear range	LOD	Reference
1.	AChE/N-CD/BSA/PGE	10–250 nM	8.6 nM	This work
2.	ITO/MnPc-TA/N3-PANI	0.20–7.50 μmol dm^{-3}	0.062 μmol dm^{-3}	[56]
3.	Au-Pt@BSA-GNRs/GCE	0.01–10.0 10.0–170 μM	2 nM	[57]
4.	Nano-MIP/CP electrode	0.1–2 μmol dm^{-3}	7.9×10^{-3} μmol dm^{-3}	[58]
5.	Micro IrO_x	100–10,000 and 10,000–1,000,000 nM	3000 nM	[59]
6.	HMDE	40–390 nM	11 nM	[60]
7.	Nafion coated GCE	0–5000 nM	75 nM	[61]

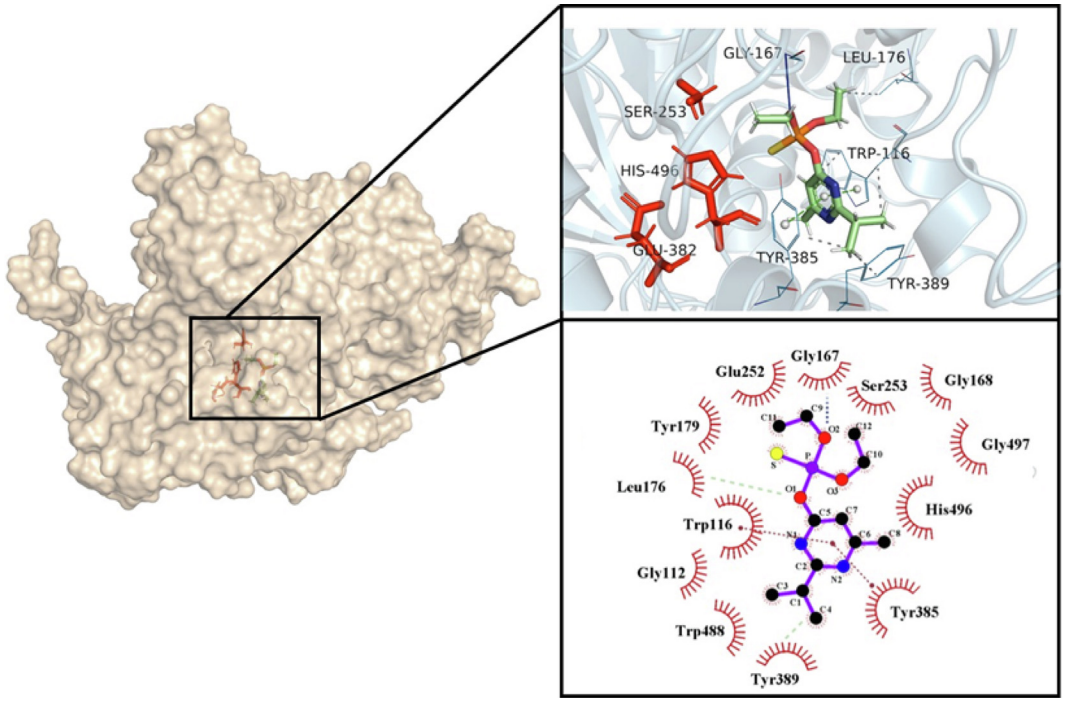

Fig. 8. Showing surface view of molecular docking of Diazinon with Honey bee AChE: upper inset shows close up view of amino acid residues of AChE interacting with diazinon where active site amino acid residues are shown in red, lower inset shows LigPlot view where the arcs with spokes radiating towards the ligand indicate hydrophobic contacts with ligand atoms, green lines show H-bonds, blue lines shows some of important hydrophobic interactions, while blue line with round cap shows p stacking interactions. (For interpretation of the references to colour in this figure legend, the reader is referred to the web version of this article.)

hydrophobic interactions are shown in Fig. 8. The most prominent interaction revealed with Leu^{176} (Fig. 8). The amino acids present in catalytic triad are shown in red. The same amino acids have been previously reported to form active site for the Am-AChE1 [63]. The authors of [64] reported the crystal structure of Honey bee AChE to determine the contact toxicity of pesticides by AChE inhibition. The binding of diazinon with Trp^{116} in the anion binding site and Gly^{167} in the oxyanion hole forming site of active site suggests irreversible binding of diazinon to the active site of enzyme. As, these residues play important role in the conformation and behavior of active site gorge therefore binding of inhibitor at these sites blocks the passage of substrate to the active site. The binding affinity and conformational behavior of enzyme-inhibitor complex acclaims toxicity of Diazinon to Am-AChE and it is evident from the results that experimental data are consistent with the computational findings. The sensitivity of honeybees to different pesticides varies depending upon factors like genetic background and insecticide resistance. Several reports have been published on impact of organophosphates on honey bees [16,65,66]. It is known that digestive and nervous system enzymes of honey bee act differently than enzymes of other social insects. Previous reports have suggested that honey bee acetylcholinesterase is not inhibited by certain organic pesticides which potently inhibit this enzyme in other insects such as *T. castaneum*. The authors in [67] reported honey bee AChE is not inhibited by neem derived saponins, moreover coumaphos and amitraz pesticides are not very toxic to honey bees and are frequently used by beekeepers [68]. The potential of insect acetylcholinesterase for the formation of pesticide biosensor has been studied previously with *T. castaneum* and its enzymes have been known to be inhibited strongly with organic as well as chemical pesticides [11]. Here we have compared the Am-AChE and Diazinon binding interactions with *T. castaneum* AChE and Diazinon (Fig. S2). The inhibitor bind with relatively high affinity with *T. castaneum* AChE and interact with Gly^{186}, Tyr^{396} through hydrogen bonding, whereas most prominent interactions include Ala^{149}, Trp^{152}, Tyr^{189} and Leu^{195}. The binding interactions with Tyr^{189} and Tyr^{396}, which renders the conformation of active site gorge to relatively open to allow binding of substrate to active site, whereas Gly^{186} is a part of oxyanion hole [69]. Therefore the Diazinon binding at these residues would change the conformation of active site making it unable to bind to the actual substrate. The results depict that the binding affinity of Diazinon with both insects is different therefore there toxicity would also be different. The results depict why there is a need to study honeybee AChE inhibition sensitivity by different OPs and establish methods to detect the presence of these pesticides in honeybees or areas where they form their colonies.

3.10. Real time application of biosensor

To test the commercial aspect of developed biosensor platform, the practicability of the integrated electrode system was tested in real samples of wheat flour following a standard addition method described previously [11]. As given in Table 2, the values of recovery percentages obtained for diazinon ranged from 97 to 99.4%. The results demonstrated that the as-prepared AChE/N-CD/BSA/PGE biosensor is reliable for detection of OPs on real agriculture samples providing high recovery rates with RSD < 5%.

3.11. Method validation

The detection specificity of the biosensor was assessed with various interfering analytes (Fig. 9A). For this purpose, the peak oxidation current value of the fabricated biosensor electrodes was recorded in PBS (0.1 M, pH = 7.4) containing 6 mM ATCl with diazinon and other interferrents. It was clear that the peak current response did not decrease significantly except in the presence of pesticide. The results highlighted a satisfactory pesticide detection specificity with the biosensor. To verify the operational stability of the biosensor independent CV measurements of five freshly prepared electrodes was taken as shown in Fig. 9B, using 6 mM ATCl and a mean peak current of 4.0 ± 5 μA was attained each time, displaying a good reproducibility of the biosensor with RSD < 3% (n = 5). Moreover, the precision of the offered biosensor was verified by the inter-assay where five fabricated biosensor electrodes were utilized to independently detect pesticide and relative stan-

Table 2
Detection of Diazinon in wheat flour samples using AChE/N-CD/BSA/PGE electrode system.

Pesticide	Added (nM)		Recovered (nM)	% Recovery	RSD
Diazinon	i.	10	9.7	97	4.7
	ii.	100	98.8	98.8	2.9
	iii.	250	249	99.4	4.0

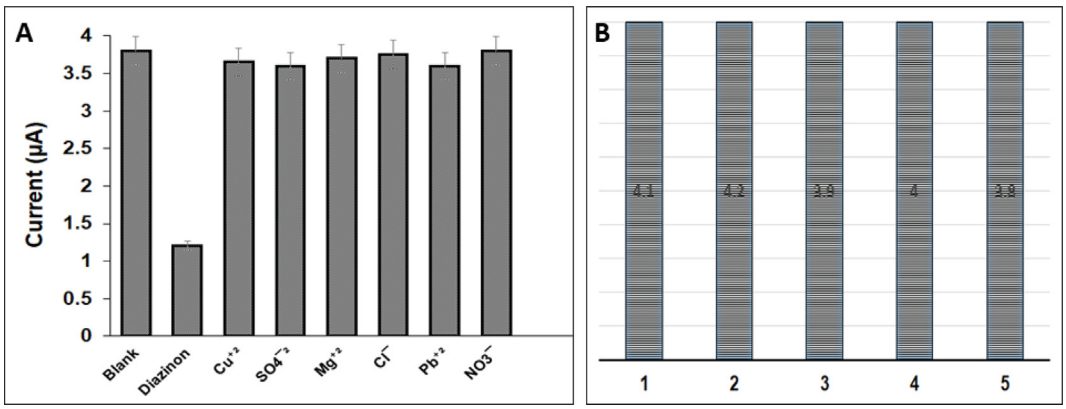

Fig. 9. (A) Analytical response of biosensor in the presence of various interferrents. (B) The oxidation peak current values recorded for five independent freshly prepared AChE/N-CD/BSA/PGE electrodes using 6 mM ATCl in 0.1 M PBS (pH = 7.4).

dard deviation (RSD) was <4.5% which corresponds to good operational stability of the as-prepared biosensor interface. Nonetheless, the storage stability of integrated bioelectrodes was determined by observing changes in the amperometric response of electrodes for over a period of 30 days by using electrodes stored at 4 °C and the current response was reduced to 50% of the original response for the same ATCI concentration.

4. Conclusion

The present study aims to explore the potential of an electrochemical test for the interpretation of organophosphorus pesticides sensitivity associated to honey bee acetylcholinesterase. To achieve this goal an acetylcholinesterase biosensor was designed utilizing Honey bee acetylcholinesterase. To improve the electroanalytical response of integrated electrodes, the mechanical and physical properties of amine rich carbon dots were utilized by integrating with BSA. The prepared nanocomposite was electrodeposited on the surface of PGE that eventually produced an effective transducer interface with enhanced electrocatalytic property and high enzyme immobilization efficiency. The nanocomposite by the virtue of its nanostructure and abundance of functional groups created a biocompatible microenvironment for the enzyme and stabilizes its biological activity by restricting its leakage from the interface. Consequently, the detection sensitivity of the proposed biosensor enhanced significantly as compared to its bare and non-doping counterparts. Besides, the inhibition activity of *A. mellifera* AChE in the presence of an OP, Diazinon was studied successfully. The biosensor also showed good linear range, high selectivity, and reliable reproducibility. In addition, the *in-silico* studies gave an insight about the contact toxicity of honey bee AChE activity by diazinon, and provided information about the interacting residues of the enzyme involved in the process of inhibition. The molecular docking analysis further validated the experimental results. The proposed interface was also tested for its applicability in agricultural food products for the determination of diazinon contamination and the results indicated a good practicability of the designed biosensor platform for wheat samples. This electrochemical method provides a sound foundation to detect target inhibitors and can be employed for honey bees as an effort to minimize the impact of non-target insecticides on honey bees and to imply good management practices in agriculture and public health policies. Future prospects may involve use of genetically engineered honey bee acetylcholinesterase for large scale production of biosensors for pesticide detection in honey, pollen and bee colonies.

Declaration of Competing Interest

The authors declare that they have no known competing financial interests or personal relationships that could have appeared to influence the work reported in this paper.

Acknowledgement

The support from the Pakistan science foundation through project PSF-MSRTII/AGR/P-COMSATS-LHR (09)/2019 and COMSATS University are gratefully acknowledged.

Appendix A. Supplementary material

Supplementary data to this article can be found online at https://doi.org/10.1016/j.bioelechem.2021.107999.

References

[1] S. Zandi, B. Nemati, D. Jahanianfard, M. Davarazar, Y. Sheikhnejad, A. Mostafaie, M. Kamali, T.M. Aminabhavi, Industrial biowastes treatment using membrane bioreactors (MBRs)-a scientometric study, J. Environ. Manage. 247 (2019) 462–473.
[2] M.T. Sohail, S. Ullah, M.T. Majeed, A. Usman, Pakistan management of green transportation and environmental pollution: a nonlinear ARDL analysis, Environ. Sci. Pollut. Res. (2021) 1–10.
[3] Š. Štěpánková, K. Vorčáková, Cholinesterase-based biosensors, J. Enzyme Inhibition Medicinal Chem. 31 (2016) 180–193.
[4] S. Soares, H. Martins, R.O. Duarte, J.J. Moura, J. Coucelo, C. Gutiérrez-Merino, M. Aureliano, Vanadium distribution, lipid peroxidation and oxidative stress markers upon decavanadate in vivo administration, J. Inorganic Biochem. 101 (2007) 80–88.
[5] J. Cao, M. Wang, H. Yu, Y. She, Z. Cao, J. Ye, A.M. Abd El-Aty, A. Hacımüftüoğlu, J. Wang, S. Lao, An Overview on the Mechanisms and Applications of Enzyme Inhibition-Based Methods for Determination of Organophosphate and Carbamate Pesticides, J. Agric. Food. Chem. 68 (2020) 7298–7315.
[6] J.R. Haigh, L.J. Lefkowitz, B.R. Capacio, B.P. Doctor, R.K. Gordon, Advantages of the WRAIR whole blood cholinesterase assay: Comparative analysis to the micro-Ellman, Test-mate ChE™, and Michel (ΔpH) assays, Chem. Biol. Interact. 175 (1-3) (2008) 417–420.
[7] L. Xiang, C. Zhao, J. Wang, Nanomaterials-based electrochemical sensors and biosensors for pesticide detection, Sensor Lett. 9 (2011) 1184–1189.
[8] N.K. Bakirhan, B. Uslu, S.A. Ozkan, The detection of pesticide in foods using electrochemical sensors, Elsevier, Food Safety and Preservation, 2018, pp. 91–141.
[9] A. Hayat, J.L. Marty, Disposable screen printed electrochemical sensors: Tools for environmental monitoring, Sensors 14 (2014) 10432–10453.
[10] W. Wang, X. Wang, N. Cheng, Y. Luo, Y. Lin, W. Xu, D. Du, Recent advances in nanomaterials-based electrochemical (bio) sensors for pesticides detection, TrAC Trends Anal. Chem. (2020) 116041.
[11] S. Bilal, M.M. Hassan, M.F. ur Rehman, M. Nasir, A.J. Sami, A. Hayat, An insect acetylcholinesterase biosensor utilizing WO3/g-C3N4 nanocomposite modified pencil graphite electrode for phosmet detection in stored grains, Food Chem. 346 (2021).
[12] N. Gallai, J.-M. Salles, J. Settele, B.E. Vaissière, Economic valuation of the vulnerability of world agriculture confronted with pollinator decline, Ecol. Econ. 68 (2009) 810–821.
[13] N.W. Calderone, Insect pollinated crops, insect pollinators and US agriculture: trend analysis of aggregate data for the period 1992–2009, PloS One 7 (2012).
[14] K. Kadlikova, M. Vaclavikova, T. Halesova, M. Kamler, M. Markovic, T. Erban, The investigation of honey bee pesticide poisoning incidents in Czechia, Chemosphere 263 (2021) 128056.
[15] K.S. Traynor, S. Tosi, K. Rennich, N. Steinhauer, E. Forsgren, R. Rose, G. Kunkel, S. Madella, D. Lopez, H. Eversole, Pesticides in honey bee colonies: Establishing a baseline for real world exposure over seven years in the USA, Environ. Pollut. 279 (2021) 116566.
[16] V. Bommuraj, Y. Chen, M. Birenboim, S. Barel, J.A. Shimshoni, Concentration- and time-dependent toxicity of commonly encountered pesticides and pesticide mixtures to honeybees (Apis mellifera L.), Chemosphere 266 (2021).
[17] B. Ionel, European regulation in the veterinary sanitary and food safety area, a component of the European policies on the safety of food products and the protection of consumer interests: A 2007 retrospective. part one: the role of European institutions in laying down and passing laws specific to the veterinary sanitary and food safety area, Revista Universul Juridic ISSN 2393-3445, (2016) 12–15.
[18] B. Ionel, European Regulation in the Veterinary Sanitary and Food Safety Area, a Component of the European Policies on the Safety of Food Products and the Protection of Consumer Interests: A 2007 Retrospective. Part Three: Directives, Universul Juridic (2016) 20–23.
[19] B. Ionel, European regulation in the veterinary sanitary and food safety area, a component of the European policies on the safety of food products and the protection of consumer interests: a 2007 retrospective. part two: regulations, Revista Universul Juridic ISSN 2393-3445, (2016) 16–19.
[20] B. Ionel, European Regulation in the Veterinary Sanitary and Food Safety Area, a Component of the European Policies on the Safety of Food Products and the Protection of Consumer Interests: A 2007 Retrospective. Part Four: Decisions, Universul Juridic (2016) 24–27.
[21] I. Hrynko, B. Łozowicka, P. Kaczyński, Development of precise micro analytical tool to identify potential insecticide hazards to bees in guttation fluid using LC–ESI–MS/MS, Chemosphere 263 (2021) 128143.
[22] D. Roy, A. Das, C.K. De, S. Mandal, P.R. Bangal, P.K. Mandal, Why Does the Photoluminescence Efficiency Depend on Excitation Energy in Case of a Quantum Dot? A Case Study of CdSe-Based Core/Alloy Shell/Shell Quantum Dots Employing Ultrafast Pump-Probe Spectroscopy and Single Particle Spectroscopy, J. Phys. Chem. 123 (2019) 6922–6933.
[23] S.P. Dharupaneedi, S.K. Nataraj, M. Nadagouda, K.R. Reddy, S.S. Shukla, T.M. Aminabhavi, Membrane-based separation of potential emerging pollutants, Separat. Purification Technol. 210 (2019) 850–866.
[24] G. Zhao, B. Zhou, X. Wang, J. Shen, B. Zhao, Detection of organophosphorus pesticides by nanogold/mercaptomethamidophos multi-residue electrochemical biosensor, Food Chem. 354 (2021) 129511.

[25] M.L. Liu, B.B. Chen, C.M. Li, C.Z. Huang, Carbon dots: synthesis, formation mechanism, fluorescence origin and sensing applications, Green Chem. 21 (2019) 449–471.
[26] A. Mehta, A. Mishra, S. Basu, N.P. Shetti, K.R. Reddy, T.A. Saleh, T.M. Aminabhavi, Band gap tuning and surface modification of carbon dots for sustainable environmental remediation and photocatalytic hydrogen production–A review, J. Environ. Manage. 250 (2019) 109486.
[27] M. Pirsaheb, S. Mohammadi, A. Salimi, Current advances of carbon dots based biosensors for tumor marker detection, cancer cells analysis and bioimaging, TrAC Trends Anal. Chem. 115 (2019) 83–99.
[28] D. Qu, Z. Sun, M. Zheng, J. Li, Y. Zhang, G. Zhang, H. Zhao, X. Liu, Z. Xie, Three Colors Emission from S, N Co-doped Graphene Quantum Dots for Visible Light H2 Production and Bioimaging, Adv. Opt. Mater. 3 (3) (2015) 360–367.
[29] S. Dey, P. Chithaiah, S. Belawadi, K. Biswas, C.N.R. Rao, New methods of synthesis and varied properties of carbon quantum dots with high nitrogen content, J. Mater. Res. 29 (3) (2014) 383–391.
[30] B.-P. Qi, L. Bao, Z.-L. Zhang, D.-W. Pang, Electrochemical methods to study photoluminescent carbon nanodots: Preparation, photoluminescence mechanism and sensing, ACS Appl. Mater. Interfaces 8 (2016) 28372–28382.
[31] M. Antonietti, N. Lopez-Salas, A. Primo, Adjusting the Structure and Electronic Properties of Carbons for Metal-Free Carbocatalysis of Organic Transformations, Adv. Mater. 31 (2019) 1805719.
[32] C. Gutiérrez-Sánchez, M. Mediavilla, T. Guerrero-Esteban, M. Revenga-Parra, F. Pariente, E. Lorenzo, Direct covalent immobilization of new nitrogen-doped carbon nanodots by electrografting for sensing applications, Carbon 159 (2020) 303–310.
[33] F. Li, D. Yang, H. Xu, Non-Metal-Heteroatom-Doped Carbon Dots: Synthesis and Properties, Chem.–A Eur. J. 25 (2019) 1165–1176.
[34] H. Li, M. Zhu, W. Chen, K. Wang, Ternary heterojunctions composed of BiOCl, BiVO 4 and nitrogen-doped carbon quantum dots for use in photoelectrochemical sensing: effective charge separation and application to ultrasensitive sensing of dopamine, Microchimica Acta 184 (2017) 4827–4833.
[35] L. Zhou, X. Zhou, C. Zhao, Y. Liu, Y. Li, L. Ma, Y. He, Y. Jiang, J. Gao, N-Doped Porous Molybdenum Carbide Nanoflowers: A Novel Sensing Platform for Organophosphorus Pesticides Detecting, Microchem. J. (2021) 106169.
[36] H. Dzudzevic Cancar, S. Soylemez, Y. Akpinar, M. Kesik, S. Göker, G. Gunbas, M. Volkan, L. Toppare, A novel acetylcholinesterase biosensor: core–shell magnetic nanoparticles incorporating a conjugated polymer for the detection of organophosphorus pesticides, ACS Appl. Mater. Interf. 8 (2016) 8058–8067.
[37] E. Krieger, G. Vriend, YASARA View—molecular graphics for all devices—from smartphones to workstations, Bioinformatics 30 (2014) 2981–2982.
[38] S. Bilal, M.M. Hassan, M.F. ur Rehman, M. Nasir, A.J. Sami, A. Hayat, An insect acetylcholinesterase biosensor utilizing WO3/g-C3N4 nanocomposite modified pencil graphite electrode for phosmet detection in stored grains, Food Chem. 346 (2021).
[39] R.A. Laskowski, M.B. Swindells, LigPlot+: multiple ligand–protein interaction diagrams for drug discovery, ACS Publications, 2011.
[40] J. Niu, H. Gao, L. Wang, S. Xin, G. Zhang, Q. Wang, L. Guo, W. Liu, X. Gao, Y. Wang, Facile synthesis and optical properties of nitrogen-doped carbon dots, New J. Chem. 38 (2014) 1522–1527.
[41] S.-L. Hu, K.-Y. Niu, J. Sun, J. Yang, N.-Q. Zhao, X.-W. Du, One-step synthesis of fluorescent carbon nanoparticles by laser irradiation, J. Mater. Chem. 19 (2009) 484–488.
[42] B. Ojha, G. Das, Role of hydrophobic and polar interactions for BSA–amphiphile composites, Chem. Phys. Lipids 164 (2011) 144–150.
[43] S. Zhu, Q. Meng, L. Wang, J. Zhang, Y. Song, H. Jin, K. Zhang, H. Sun, H. Wang, B. Yang, Highly photoluminescent carbon dots for multicolor patterning, sensors, and bioimaging, Angew. Chem. 125 (2013) 4045–4049.
[44] J. Ge, Y. Shen, W. Wang, Y. Li, Y. Yang, N-doped carbon dots for highly sensitive and selective sensing of copper ion and sulfide anion in lake water, J. Environ. Chem. Eng. 9 (2021).
[45] K.M. Omer, K.H.H. Aziz, Y.M. Salih, D.I. Tofiq, A.Q. Hassan, Photoluminescence enhancement via microwave irradiation of carbon quantum dots derived from solvothermal synthesis of L-arginine, New J. Chem. 43 (2019) 689–695.
[46] S.B. Aziz, A.Q. Hassan, S.J. Mohammed, W.O. Karim, M. FZ Kadir, H.A. Tajuddin, N. NMY Chan, Structural and optical characteristics of PVA: C-Dot composites: Tuning the absorption of ultra violet (UV) region, Nanomaterials 9 (2019) 216.
[47] D. Ghosh, S. Mondal, S. Ghosh, A. Saha, Protein conformation driven biomimetic synthesis of semiconductor nanoparticles, J. Mater. Chem. 22 (2012) 699–706.
[48] Q. Wang, Y. Kuo, Y. Wang, G. Shin, C. Ruengruglikit, Q. Huang, Luminescent properties of water-soluble denatured bovine serum albumin-coated CdTe quantum dots, J. Phys. Chem. B 110 (2006) 16860–16866.
[49] Y.-X. Li, J.-Y. Lee, H. Lee, C.-C. Hu, T.-C. Chiu, Highly fluorescent nitrogen-doped carbon dots for selective and sensitive detection of Hg2+ and ClO− ions and fluorescent ink, J. Photochem. Photobiol. A: Chem. 405 (2021).
[50] A. Hayat, L. Barthelmebs, A. Sassolas, J.-L. Marty, An electrochemical immunosensor based on covalent immobilization of okadaic acid onto screen printed carbon electrode via diazotization-coupling reaction, Talanta 85 (2011) 513–518.
[51] M.H. Nawaz, A. Hayat, G. Catanante, U. Latif, J.L. Marty, Development of a portable and disposable NS1 based electrochemical immunosensor for early diagnosis of dengue virus, Analytica Chim. Acta 1026 (2018) 1–7.
[52] H.-F. Cui, T.-T. Zhang, Q.-Y. Lv, X. Song, X.-J. Zhai, G.-G. Wang, Bioelectronics, An acetylcholinesterase biosensor based on doping Au nanorod@ SiO2 nanoparticles into TiO2-chitosan hydrogel for detection of organophosphate pesticides, Biosensors Bioelectron. 141 (2019) 111452.
[53] B. Wang, Y. Li, H. Hu, W. Shu, L. Yang, J. Zhang, Acetylcholinesterase electrochemical biosensors with graphene-transition metal carbides nanocomposites modified for detection of organophosphate pesticides, PloS One 15 (2020).
[54] Y. Yang, Y. Zhao, F. Sun, T. You, Y. Gao, P. Yin, Electrochemically synthesized superhydrophilic 3D tree-like Ag microstructure for ultrasensitive detection of omethoate, Microchem. J. 159 (2020) 105427.
[55] M. Kesik, F.E. Kanik, J. Turan, M. Kolb, S. Timur, M. Bahadir, L. Toppare, An acetylcholinesterase biosensor based on a conducting polymer using multiwalled carbon nanotubes for amperometric detection of organophosphorous pesticides, Sens. Actuators, B 205 (2014) 39–49.
[56] D. Akyüz, A. Koca, An electrochemical sensor for the detection of pesticides based on the hybrid of manganese phthalocyanine and polyaniline, Sensors Actuators B: Chem. 283 (2019) 848–856.
[57] N. Pajooheshpour, M. Rezaei, A. Hajian, A. Afkhami, M. Sillanpää, F. Arduini, H. Bagheri, Protein templated Au-Pt nanoclusters-graphene nanoribbons as a high performance sensing layer for the electrochemical determination of diazinon, Sensors Actuators B: Chem. 275 (2018) 180–189.
[58] A. Motaharian, F. Motaharian, K. Abnous, M.R.M. Hosseini, M. Hassanzadeh-Khayyat, Molecularly imprinted polymer nanoparticles-based electrochemical sensor for determination of diazinon pesticide in well water and apple fruit samples, Analy. Bioanal. Chem. 408 (2016) 6769–6779.
[59] J. Wang, M. Yokokawa, T. Satake, H. Suzuki, A micro IrOx potentiometric sensor for direct determination of organophosphate pesticides, Sensors Actuat. B: Chem. 220 (2015) 859–863.
[60] D. Guziejewski, S. Skrzypek, W. Ciesielski, Square wave adsorptive stripping voltammetric determination of diazinon in its insecticidal formulations, Environ. Monitoring Assess. 184 (2012) 6575–6582.
[61] G. Erdoğdu, A sensitive voltammetric method for the determination of diazinon insecticide, J. Anal. Chem. 58 (2003) 569–572.
[62] M.B. Colović, D.Z. Krstić, T.D. Lazarević-Pašti, A.M. Bondžić, V.M. Vasić, Acetylcholinesterase inhibitors: pharmacology and toxicology, Curr Neuropharmacol 11 (2013) 315–335.
[63] Y.H. Kim, D.J. Cha, J.W. Jung, H.W. Kwon, S.H. Lee, Molecular and kinetic properties of two acetylcholinesterases from the western honey bee, Apis mellifera, PLoS One 7 (2012), e48838–e48838.
[64] F. Dulin, M.-P. Halm-Lemeille, S. Lozano, A. Lepailleur, J. Sopkova-de Oliveira Santos, S. Rault, R. Bureau, Interpretation of honeybees contact toxicity associated to acetylcholinesterase inhibitors, Ecotoxicol. Environ. Safety 79 (2012) 13–21.
[65] Y. Al Naggar, G. Codling, A. Vogt, E. Naiem, M. Mona, A. Seif, J.P. Giesy, Organophosphorus insecticides in honey, pollen and bees (Apis mellifera L.) and their potential hazard to bee colonies in Egypt, Ecotoxicol. Environ. Saf. 114 (2015) 1–8.
[66] A.D. Noi, S. Casini, T. Campani, G. Cai, I. Caliani, Review on sublethal effects of environmental contaminants in honey bees (Apis mellifera), knowledge gaps and future perspectives, Int. J. Environ. Res. Public Health 18 (2021) 1863.
[67] A.J. Sami, S. Bilal, M. Khalid, M.T. Nazir, A. Shakoori, A Comparative Study of Inhibitory Properties of Saponins (derived from Azadirachta indica) for Acetylcholinesterase of Tribolium castaneum and Apis mellifera, Pakistan, J. Zool. 50 (2018) 725–733.
[68] F.D. Rinkevich, J.W. Margotta, J.M. Pittman, R.G. Danka, M.R. Tarver, J.A. Ottea, K.B.J.P.O. Healy, Genetics, synergists, and age affect insecticide sensitivity of the honey bee, Apis mellifera 10 (2015).
[69] Y. Lu, Y.-P. Pang, Y. Park, X. Gao, J. Yao, X. Zhang, K.Y. Zhu, Genome organization, phylogenies, expression patterns, and three-dimensional protein models of two acetylcholinesterase genes from the red flour beetle, PLoS One 7 (2012).